10 March 2000

ELSEVIER

Chemical Physics Letters 319 (2000) 27–44

CHEMICAL PHYSICS LETTERS

www.elsevier.nl/locate/cplett

Semiclassical initial value representation techniques for chaotic systems

B.R. McQuarrie [1], Paul Brumer [*]

Chemical Physics Theory Group, Department of Chemistry, University of Toronto, Toronto, ONT M5S 3H6, Canada

Received 8 November 1999; in final form 28 December 1999

Abstract

Semiclassical wavefunction propagation for chaotic systems suffer from numerical difficulties due to the chaotic nature of classical trajectories, resulting in reduced accuracy for standard initial value representation (IVR) methods. We compare four recent IVR methods developed to overcome these difficulties (Herman–Kluk with trajectory truncation; stationary-phase Herman–Kluk (SPHK); cellularized frozen Gaussian approximation; stationary-phase Monte Carlo) by computing the Franck–Condon spectrum of the 2-dimensional Henon–Heiles and quartic oscillator systems. The SPHK is found to be the most successful of the four methods. The SPHK is then used to determine the spectrum for collinear CO_2 photodissociation.

1. Introduction

There has been a great deal of recent interest in semiclassical methods to treat the dynamics of atoms and molecules based upon an initial value representation (IVR) [1–7]. An IVR expresses the system dynamics as an integral over initial phase-space (coordinate and momenta) variables. Dynamical system quantities are evaluated along the classical trajectories which emanate from these initial phase-space points. The primary advantage of IVR methods is that they do not require a search for trajectories which satisfy both initial and final time constraints, which is the case for any boundary value representation such as the Van Vleck propagator [8]. The central deficiency of IVR methods is in the need to integrate over highly oscillatory integrands. Here we examine IVR propagators for the numerically difficult case of chaotic dynamics.

Extensive studies have been carried out to compare IVR propagators for non-chaotic systems. In this case, the Herman–Kluk (HK) frozen Gaussian approximation [2], an improved version of the original frozen Gaussian approximation of Heller [1], has proven particularly useful. In addition to providing reliable results, the method does not require the computation of the Maslov index [5], a simplifying feature. For example, Kay compared several IVR methods for non-chaotic systems [4], and concluded that the HK propagator can produce highly accurate results which converge quickly. Similarly, Garashchuk and Tannor [9] found the HK formalism to be far better at treating reactive scattering than other semiclassical methods, and van de Sand and

* Corresponding author. Fax: (416) 978-5325; e-mail: pbrumer@tikva.chem.utoronto.ca

[1] E-mail: bmcquar@tikva.chem.utoronto.ca

0009-2614/00/$ - see front matter
PII: S0009-2614(00)00053-1

Rost [10] successfully treated 3-dimensional Coulomb scattering using the HK propagator. This propagator has also been used by Walton and Manolopoulos to treat collinear CO_2 photodissociation [11] (cf. Section 3). The method converged but required 10^8 trajectories. The large number of trajectories is undoubtably due to the dissociative nature of the problem, but the authors also identified unstable periodic orbits as a contributing factor.

Far fewer studies have been directed at chaotic dynamics. Here chaotic trajectories and associated exponential growth cause serious convergence problems for the oscillatory integrals that dominate IVR methods. Kay treated bound chaotic systems [12] and noted that the HK method was not very successful due to chaotic trajectories which caused the integrand to grow exponentially. To resolve this problem Kay proposed discarding excessively unstable trajectories, an ad hoc procedure (which we term HKK) that produced good results. Subsequently, Campolieti and Brumer [13] introduced a stationary-phase approach that automatically weighted chaotic trajectories, obviating the need for arbitrary truncation of any trajectories. The resultant technique, a stationary-phase Monte Carlo (SPMC) not related to the HK approach, provided good results for bound chaotic dynamics.

Attempts have also been made to modify the HK integral to treat chaotic dynamics. We examine two such methods: the stationary-phase Herman–Kluk (SPHK) of Herman [7] and the cellularized frozen Gaussian approximation (CFGA) of Walton and Manolopoulos [6]. In this Letter, we will consider these three modified HK methods (HKK, SPHK, and CFGA) and compare their utility on a number of chaotic systems. We also include a comparison with our previously proposed stationary-phase Monte Carlo (SPMC) method [13]. Comparisons are made by computing the Franck–Condon spectrum for three 2-dimensional systems of varying degrees of chaotic behavior (Henon-Heiles (HH) and quartic oscillator potential). Our goal is to assess both accuracy and to determine the method which requires the fewest trajectories for convergence. The results are compared, and the SPHK approach is found to be the most successful. This method is then used to treat collinear CO_2 photodissociation. We show that the SPHK method can obtain reasonable estimates of the spectrum using orders of magnitude fewer trajectories than the unmodified HK approach.

Note that the systems we consider have been examined previously by some type of semiclassical IVR method (Henon–Heiles in Ref. [6]; quartic oscillator in Refs. [12,13]; collinear CO_2 in Ref. [11]). However, this Letter provides a systematic comparison of the methods, crucial to further development of this area. A comparison of the IVR methods applied to chaotic systems, as presented in this Letter, leads to the unambiguous conclusion that the SPHK is the best of the four approaches for the properties studied.

2. Semiclassical propagation of wavefunctions

In Section 2, we outline the Franck–Condon spectral theory, and describe the four IVR procedures.

The absorption spectrum $I(E)$, the quantity we wish to compute, can be expressed as the Fourier transform of an autocorrelation function [14]

$$I(E) = \mathrm{Re}\frac{1}{2\pi\hbar}\int_{-\infty}^{\infty} \mathrm{d}t \exp(iEt/\hbar) C(t), \tag{1}$$

where $C(t) = \langle \Psi_0 | \exp(-i\hat{H}t/\hbar) | \Psi_0 \rangle$ is the autocorrelation function for an initial Ψ_0 propagating under Hamiltonian $\hat{H}$. The initial state is chosen to be a Gaussian in the coordinate representation

$$\Psi_0(\boldsymbol{q}') = \langle \boldsymbol{q}' | \bar{\boldsymbol{p}}\bar{\boldsymbol{q}}\alpha 0 \rangle \equiv (2\alpha/\pi)^{d/4} \times \exp\left(-\alpha|\boldsymbol{q}' - \bar{\boldsymbol{q}}|^2 + i\bar{\boldsymbol{p}}\cdot(\boldsymbol{q}' - \bar{\boldsymbol{q}})/\hbar\right), \tag{2}$$

where $\bar{\boldsymbol{q}}$ and $\bar{\boldsymbol{p}}$ are the coordinate and momentum shift, respectively, and α is a width parameter. The $(\boldsymbol{q},\boldsymbol{p})$ phase space is of dimension $2d$.

A wavefunction at time t is given in terms of the wavefunction at time zero by

$$\Psi_t(\boldsymbol{x}) = \int \mathrm{d}\boldsymbol{x}' K_t(\boldsymbol{x},\boldsymbol{x}') \Psi_0(\boldsymbol{x}'), \tag{3}$$

where $K_t(\boldsymbol{x},\boldsymbol{x}')$ is the Feynman propagator

$$K_t(\boldsymbol{x},\boldsymbol{x}') = \langle \boldsymbol{x} | \exp\left(-i\hat{H}t/\hbar\right) | \boldsymbol{x}' \rangle. \tag{4}$$

The autocorrelation function is therefore given by

$$C(t) = \int \mathrm{d}\boldsymbol{x}\, \Psi_0^*(\boldsymbol{x}) \int \mathrm{d}\boldsymbol{x}'\, K_t(\boldsymbol{x},\boldsymbol{x}')\, \Psi_0(\boldsymbol{x}'). \quad (5)$$

A semiclassical approximation to the quantum wavefunction at t is obtained by replacing K_t by a semiclassical propagator K_t^{sc}, giving the semiclassical approximation $C^{\mathrm{sc}}(t)$ to the autocorrelation function.

2.1. Herman–Kluk propagator

To appreciate the differences between the semiclassical propagators, we consider the structure of each method studied. The HK propagator is given by [3]

$$K_t^{\mathrm{sc}}(\boldsymbol{x},\boldsymbol{x}') = \frac{1}{(2\pi\hbar)^d} \int \mathrm{d}\boldsymbol{p} \int \mathrm{d}\boldsymbol{q}\, R_{\boldsymbol{p}\boldsymbol{q}t}\, \mathrm{e}^{iS_{\boldsymbol{p}\boldsymbol{q}t}/\hbar} \times \langle \boldsymbol{x}|\boldsymbol{p}(t)\boldsymbol{q}(t)\alpha' 0\rangle \langle \boldsymbol{p}\boldsymbol{q}\alpha' 0|\boldsymbol{x}'\rangle, \quad (6)$$

where

$$S_{\boldsymbol{p}\boldsymbol{q}t} = \int_0^t \mathrm{d}t'\, \boldsymbol{p}(t') \cdot \dot{\boldsymbol{q}}(t') - H(\boldsymbol{p}(t'),\boldsymbol{q}(t')), \quad (7)$$

$$R_{\boldsymbol{p}\boldsymbol{q}t} = \pm \left\{ \det\left[\tfrac{1}{2}\left(\boldsymbol{M}_{\boldsymbol{p}\boldsymbol{p}} + \boldsymbol{M}_{\boldsymbol{q}\boldsymbol{q}} - 2i\alpha'\hbar \boldsymbol{M}_{\boldsymbol{q}\boldsymbol{p}} + \frac{i}{2\alpha'\hbar} \boldsymbol{M}_{\boldsymbol{p}\boldsymbol{q}} \right) \right] \right\}^{\frac{1}{2}}. \quad (8)$$

Here $\boldsymbol{q},\boldsymbol{p}$ denote phase-space points at $t = 0$, which evolve classically to $\boldsymbol{q}(t),\boldsymbol{p}(t)$ at time t. The stability matrix $\boldsymbol{M}$ consists of the sub-matrices given by $\boldsymbol{M}_{\boldsymbol{q}\boldsymbol{q}} = \partial\boldsymbol{q}(t)/\partial\boldsymbol{q}$, $\boldsymbol{M}_{\boldsymbol{q}\boldsymbol{p}} = \partial\boldsymbol{q}(t)/\partial\boldsymbol{p}$, $\boldsymbol{M}_{\boldsymbol{p}\boldsymbol{q}} = \partial\boldsymbol{p}(t)/\partial\boldsymbol{q}$, $\boldsymbol{M}_{\boldsymbol{p}\boldsymbol{p}} = \partial\boldsymbol{p}(t)/\partial\boldsymbol{p}$. The sign of the prefactor $R_{\boldsymbol{p}\boldsymbol{q}t}$ is chosen to keep $R_{\boldsymbol{p}\boldsymbol{q}t}$ differentiable at all times. Note that the Maslov index does not appear in Eq. (6); instead $R_{\boldsymbol{p}\boldsymbol{q}t}$ must be kept differentiable over the entire trajectory.

The quantity α' (Eq. (6)) is an adjustable parameter [3], which defines the width of the frozen Gaussians which are propagated [15]. The effect of varying α' has been examined by Kay [4] for the HK, who recommends determining α' by examining energy conservation of a wavepacket, and by Herman [7]. Below, we take $\alpha' = \alpha$ for the initial wavefunction, a reasonable choice used in many cases [6,9,11,12,16].

Substituting Eqs. (2) and (6) into Eq. (5) and performing the $\boldsymbol{x}$ and $\boldsymbol{x}'$ integrations gives the HK representation of the autocorrelation function

$$C_{\mathrm{HK}}^{\mathrm{sc}}(t) = \left(\frac{1}{2\pi\hbar}\right)^d \int\int \mathrm{d}\boldsymbol{p}\, d\boldsymbol{q}\, R_{\boldsymbol{p}\boldsymbol{q}t}\, \mathrm{e}^{iS_{\boldsymbol{p}\boldsymbol{q}t}/\hbar} \times \exp\left[-\frac{\alpha}{2}(\boldsymbol{q}(t) - \bar{\boldsymbol{q}})^2 - \frac{i}{2\hbar}(\boldsymbol{p}(t) + \bar{\boldsymbol{p}}) \cdot (\boldsymbol{q}(t) - \bar{\boldsymbol{q}}) - \frac{(\boldsymbol{p}(t) - \bar{\boldsymbol{p}})^2}{8\alpha\hbar^2} \right] \exp\left[-\frac{\alpha}{2}(\boldsymbol{q} - \bar{\boldsymbol{q}})^2 + \frac{i}{2\hbar}(\boldsymbol{p} + \bar{\boldsymbol{p}}) \cdot (\boldsymbol{q} - \bar{\boldsymbol{q}}) - \frac{(\boldsymbol{p} - \bar{\boldsymbol{p}})^2}{8\alpha\hbar^2} \right]. \quad (9)$$

Eq. (9) is the unmodified version of the HK method which has been used successfully to treat non-chaotic systems [4,9–11]. The integrand in Eq. (9) is highly oscillatory due to rapid variations of the phase, and $R_{\boldsymbol{p}\boldsymbol{q}t}$ can grow exponentially fast for chaotic trajectories. For these reasons Eq. (9) is unable to provide accurate spectral estimates for chaotic systems.

A simple, surprisingly successful method [12] to treat chaotic systems using the HK propagator is to truncate trajectories when the prefactor $R_{\boldsymbol{p}\boldsymbol{q}t}$ grows large (HKK). In particular, contributions to the integral are kept until $|R_{\boldsymbol{p}\boldsymbol{q}t}|^2 > D_t$, where D_t is some arbitrarily defined function of time.

More systematic methods involve pre-averaging the integrand to reduce the oscillatory behavior [6,7,16–20], e.g. by application of a Filinov transform [21]. In a particular Filinov transformation [7], the oscillatory $2d$-dimensional integral

$$I = \int \mathrm{d}\boldsymbol{z} A(\boldsymbol{z}) \exp[if(\boldsymbol{z})], \quad (10)$$

is replaced by the approximation

$$I \sim I_\epsilon = \int \mathrm{d}\boldsymbol{z} A(\boldsymbol{z}) \exp[if(\boldsymbol{z})] \exp\left[-\epsilon |\nabla f(\boldsymbol{z})|^2 \right]. \quad (11)$$

This form emphasizes regions of stationary phase in the integral, and contains the adjustable parameter ϵ.

In general, $\lim_{\epsilon \to 0} I_\epsilon = I$, and I_ϵ approaches, as $\epsilon \to \infty$, the result of summing over stationary-phase points [17,18]. For computational purposes, ϵ should be chosen relatively small so that the series expansions used in developing I_ϵ are valid [18]. However, it is desirable to use large ϵ, since fewer trajectories are needed to converge I_ϵ. Unfortunately, as $\epsilon \to \infty$, determining the stationary-phase points becomes increasingly difficult, and any brute force numerical implementation is bound to fail. These considerations are used to determine a suitable ϵ; the converged Monte Carlo integral should be stable for a range of non-zero ϵ. This range is typically 3–4 orders of magnitude.

2.2. Stationary-phase Herman–Kluk approach

Applying Eq. (11) to Eq. (9), gives the first-order SPHK approximation [7,16,20]

$$\begin{aligned} C^{\mathrm{sc}}_{\mathrm{SPHK}}(t) = \left(\frac{1}{2\pi\hbar}\right)^d \int\int \mathrm{d}\boldsymbol{p}\,d\boldsymbol{q} R_{\boldsymbol{p}\boldsymbol{q}t} \mathrm{e}^{iS_{\boldsymbol{p}\boldsymbol{q}t}/\hbar} D_{\epsilon \boldsymbol{p}\boldsymbol{q}t} \\ \times \exp\Bigg[-\frac{\alpha}{2}\left(\boldsymbol{q}(t) - \bar{\boldsymbol{q}}\right)^2 \\ - \frac{i}{2\hbar}\left(\boldsymbol{p}(t) + \bar{\boldsymbol{p}}\right)\cdot\left(\boldsymbol{q}(t) - \bar{\boldsymbol{q}}\right) \\ - \frac{\left(\boldsymbol{p}(t) - \bar{\boldsymbol{p}}\right)^2}{8\alpha\hbar^2} \Bigg] \exp\Bigg[-\frac{\alpha}{2}\left(\boldsymbol{q} - \bar{\boldsymbol{q}}\right)^2 \\ + \frac{i}{2\hbar}\left(\boldsymbol{p} + \bar{\boldsymbol{p}}\right)\cdot\left(\boldsymbol{q} - \bar{\boldsymbol{q}}\right) - \frac{\left(\boldsymbol{p} - \bar{\boldsymbol{p}}\right)^2}{8\alpha\hbar^2} \Bigg], \end{aligned} \tag{12}$$

where

$$\begin{aligned} D_{\epsilon \boldsymbol{p}\boldsymbol{q}t} = \exp\Bigg\{ -\frac{\epsilon}{4\hbar^2} + \Big[\left(\boldsymbol{M}_{\boldsymbol{q}\boldsymbol{q}}\cdot\left(\boldsymbol{p}(t) - \bar{\boldsymbol{p}}\right) - \boldsymbol{M}_{\boldsymbol{p}\boldsymbol{q}}\right. \\ \left.\cdot\left(\boldsymbol{q}(t) - \bar{\boldsymbol{q}}\right) - \boldsymbol{p} + \bar{\boldsymbol{p}}\right)^2 \left(\boldsymbol{M}_{\boldsymbol{q}\boldsymbol{p}}\cdot\left(\boldsymbol{p}(t) - \bar{\boldsymbol{p}}\right)\right. \\ \left. - \boldsymbol{M}_{\boldsymbol{p}\boldsymbol{p}}\cdot\left(\boldsymbol{q}(t) - \bar{\boldsymbol{q}}\right) + \boldsymbol{q} - \bar{\boldsymbol{q}}\right)^2 \Big] \Bigg\}. \end{aligned} \tag{13}$$

2.3. Cellularized frozen Gaussian approach

Another method based on the Filinov transformation, is the cellularized frozen Gaussian approximation (CFGA) of Walton and Manolopoulos [6]. Since the expansions used in deriving the CFGA are to a higher order than those used for the SPHK, it is possible that the CFGA will be able to obtain the correct result for larger ϵ, and hence require fewer trajectories.

The CFGA result is [6]

$$\begin{aligned} C^{\mathrm{sc}}_{\mathrm{CFGA}}(t) = \left(\frac{1}{2\pi\hbar}\right)^d \int\int \mathrm{d}\boldsymbol{p}\,d\boldsymbol{q} R_{\boldsymbol{p}\boldsymbol{q}t} \mathrm{e}^{iS_{\boldsymbol{p}\boldsymbol{q}t}/\hbar} \\ \times \left(\frac{(4\epsilon)^{-2d}}{\det\left[\boldsymbol{A}_{\boldsymbol{p}\boldsymbol{q}t}\right]} \right)^{1/2} \\ \times \exp\left(\tfrac{1}{4}\boldsymbol{b}^T_{\boldsymbol{p}\boldsymbol{q}t} \boldsymbol{A}^{-1}_{\boldsymbol{p}\boldsymbol{q}t} \boldsymbol{b}_{\boldsymbol{p}\boldsymbol{q}t} - c_{\boldsymbol{p}\boldsymbol{q}t} \right), \end{aligned} \tag{14}$$

where

$$\boldsymbol{A}_{\boldsymbol{p}\boldsymbol{q}t} = \begin{pmatrix} \boldsymbol{A}_{\boldsymbol{q}\boldsymbol{q}} & \boldsymbol{A}_{\boldsymbol{q}\boldsymbol{p}} \\ \boldsymbol{A}_{\boldsymbol{p}\boldsymbol{q}} & \boldsymbol{A}_{\boldsymbol{p}\boldsymbol{p}} \end{pmatrix} \tag{15}$$

$$\begin{aligned} \boldsymbol{A}_{\boldsymbol{q}\boldsymbol{q}} = \frac{\alpha}{2}\boldsymbol{M}^T_{\boldsymbol{q}\boldsymbol{q}}\boldsymbol{M}_{\boldsymbol{q}\boldsymbol{q}} + \frac{1}{8\alpha\hbar^2}\boldsymbol{M}^T_{\boldsymbol{p}\boldsymbol{q}}\boldsymbol{M}_{\boldsymbol{p}\boldsymbol{q}} \\ + \left(\frac{\alpha}{2} + \frac{1}{4\epsilon}\right)\boldsymbol{I}, \end{aligned} \tag{16}$$

$$\boldsymbol{A}_{\boldsymbol{q}\boldsymbol{p}} = \frac{\alpha}{2}\boldsymbol{M}^T_{\boldsymbol{q}\boldsymbol{q}}\boldsymbol{M}_{\boldsymbol{q}\boldsymbol{p}} + \frac{1}{8\alpha\hbar^2}\boldsymbol{M}^T_{\boldsymbol{p}\boldsymbol{q}}\boldsymbol{M}_{\boldsymbol{p}\boldsymbol{p}}, \tag{17}$$

$$\boldsymbol{A}_{\boldsymbol{p}\boldsymbol{q}} = \frac{\alpha}{2}\boldsymbol{M}^T_{\boldsymbol{q}\boldsymbol{p}}\boldsymbol{M}_{\boldsymbol{q}\boldsymbol{q}} + \frac{1}{8\alpha\hbar^2}\boldsymbol{M}^T_{\boldsymbol{p}\boldsymbol{p}}\boldsymbol{M}_{\boldsymbol{p}\boldsymbol{q}}, \tag{18}$$

$$\begin{aligned} \boldsymbol{A}_{\boldsymbol{p}\boldsymbol{p}} = \frac{\alpha}{2}\boldsymbol{M}^T_{\boldsymbol{q}\boldsymbol{p}}\boldsymbol{M}_{\boldsymbol{q}\boldsymbol{p}} + \frac{1}{8\alpha\hbar^2}\boldsymbol{M}^T_{\boldsymbol{p}\boldsymbol{p}}\boldsymbol{M}_{\boldsymbol{p}\boldsymbol{p}} \\ + \left(\frac{1}{8\alpha\hbar^2} + \frac{1}{4\epsilon}\right)\boldsymbol{I}, \end{aligned} \tag{19}$$

$$\boldsymbol{b}_{\boldsymbol{p}\boldsymbol{q}t} = \begin{pmatrix} \boldsymbol{b}_{\boldsymbol{q}} \\ \boldsymbol{b}_{\boldsymbol{p}} \end{pmatrix}, \tag{20}$$

$$\boldsymbol{b}_q = \alpha\Big[\boldsymbol{M}_{qq}^T(\boldsymbol{q}(t)-\bar{\boldsymbol{q}}) + (\boldsymbol{q}-\bar{\boldsymbol{q}})\Big] + \frac{1}{4\alpha\hbar^2}\Big[\boldsymbol{M}_{pq}^T(\boldsymbol{p}(t)-\bar{\boldsymbol{p}})\Big] + \frac{i}{2\hbar}\Big[\boldsymbol{M}_{pq}^T(\boldsymbol{q}(t)-\bar{\boldsymbol{q}}) - \boldsymbol{M}_{qq}(\boldsymbol{p}(t)-\bar{\boldsymbol{p}}) + (\boldsymbol{p}-\bar{\boldsymbol{p}})\Big], \tag{21}$$

$$\boldsymbol{b}_p = \alpha\Big[\boldsymbol{M}_{qp}^T(\boldsymbol{q}(t)-\bar{\boldsymbol{q}})\Big] + \frac{1}{4\alpha\hbar^2}\times\Big[\boldsymbol{M}_{pp}^T(\boldsymbol{p}(t)-\bar{\boldsymbol{p}}) + (\boldsymbol{p}-\bar{\boldsymbol{p}})\Big] + \frac{i}{2\hbar}\Big[\boldsymbol{M}_{pp}^T(\boldsymbol{q}(t)-\bar{\boldsymbol{q}}) - \boldsymbol{M}_{qp}(\boldsymbol{p}(t)-\bar{\boldsymbol{p}}) - (\boldsymbol{q}-\bar{\boldsymbol{q}})\Big], \tag{22}$$

$$c_{\boldsymbol{p}\boldsymbol{q}t} = \frac{\alpha}{2}\Big[(\boldsymbol{q}(t)-\bar{\boldsymbol{q}})^2 + (\boldsymbol{q}-\bar{\boldsymbol{q}})^2\Big] + \frac{1}{8\alpha\hbar^2}\Big[(\boldsymbol{p}(t)-\bar{\boldsymbol{p}})^2 + (\boldsymbol{p}-\bar{\boldsymbol{p}})^2\Big] + \frac{i}{2\hbar}\Big[(\boldsymbol{p}(t)+\bar{\boldsymbol{p}})^T(\boldsymbol{q}(t)-\bar{\boldsymbol{q}}) - (\boldsymbol{p}+\bar{\boldsymbol{p}})^T(\boldsymbol{q}-\bar{\boldsymbol{q}})\Big]. \tag{23}$$

Although the CFGA introduces significant numerical complexity, it has been used successfully to treat 2- and 3-dimensional bound-state systems [6], and to obtain the photodissociation spectrum of Ar_nI^- [22].

2.4. Stationary-phase Monte Carlo

A non-HK-based propagator can also be used. We consider the method of Campolieti and Brumer [13] which uses the first-order stationary-phase method applied to the coordinate-based expression for $C(t)$. Methods of this type have been successfully used to treat both non-chaotic and chaotic systems [4,13,19,23]. This coordinate propagator yields the following result for the autocorrelation function [5]

$$C^{\mathrm{sc}}(t) = \left(\frac{1}{2\pi i\hbar}\right)^{d/2} \times \int\int \mathrm{d}\boldsymbol{p}\,\mathrm{d}\boldsymbol{q}\,|\det \boldsymbol{M}_{\boldsymbol{q}\boldsymbol{p}}|^{1/2} \mathrm{e}^{iS_{\boldsymbol{p}\boldsymbol{q}t}/\hbar} \mathrm{e}^{i\pi\nu/2} \times \Psi_0^*(\boldsymbol{q})\,\Psi_0(\boldsymbol{q}(t)), \tag{24}$$

Table 1
Numerical details associated with the spectra in Figs. 1–3 for the three systems studied

	Parameters	Number of trajectories	Average (t_f)	Trajectories truncated
HH Case 1				
SPHK	$\epsilon = 10^{-3}$	2000	428	0
SPMC	$\epsilon = 10^{-2}$	10000	428	0
CFGA	$\epsilon = 10^{-3}$	2000	421	8
HKK	$D_t = 5000$	2000	374	24
HH Case 2				
SPHK	$\epsilon = 10^{-4}$	40000	304	0
SPMC	$\epsilon = 10^{-3}$	80000	304	0
CFGA	$\epsilon = 10^{-4}$	40000	241	32
HKK	$D_t = 1000$	40000	133	71
Quartic oscillator				
SPHK	$\epsilon = 10^{-6}$	100000	50	0
SPMC	$\epsilon = 10^{-5}$	200000	50	0
CFGA	$\epsilon = 10^{-5}$	100000	6	100
HKK	$D_t = 100\mathrm{e}^{0.2t}$	100000	6	99

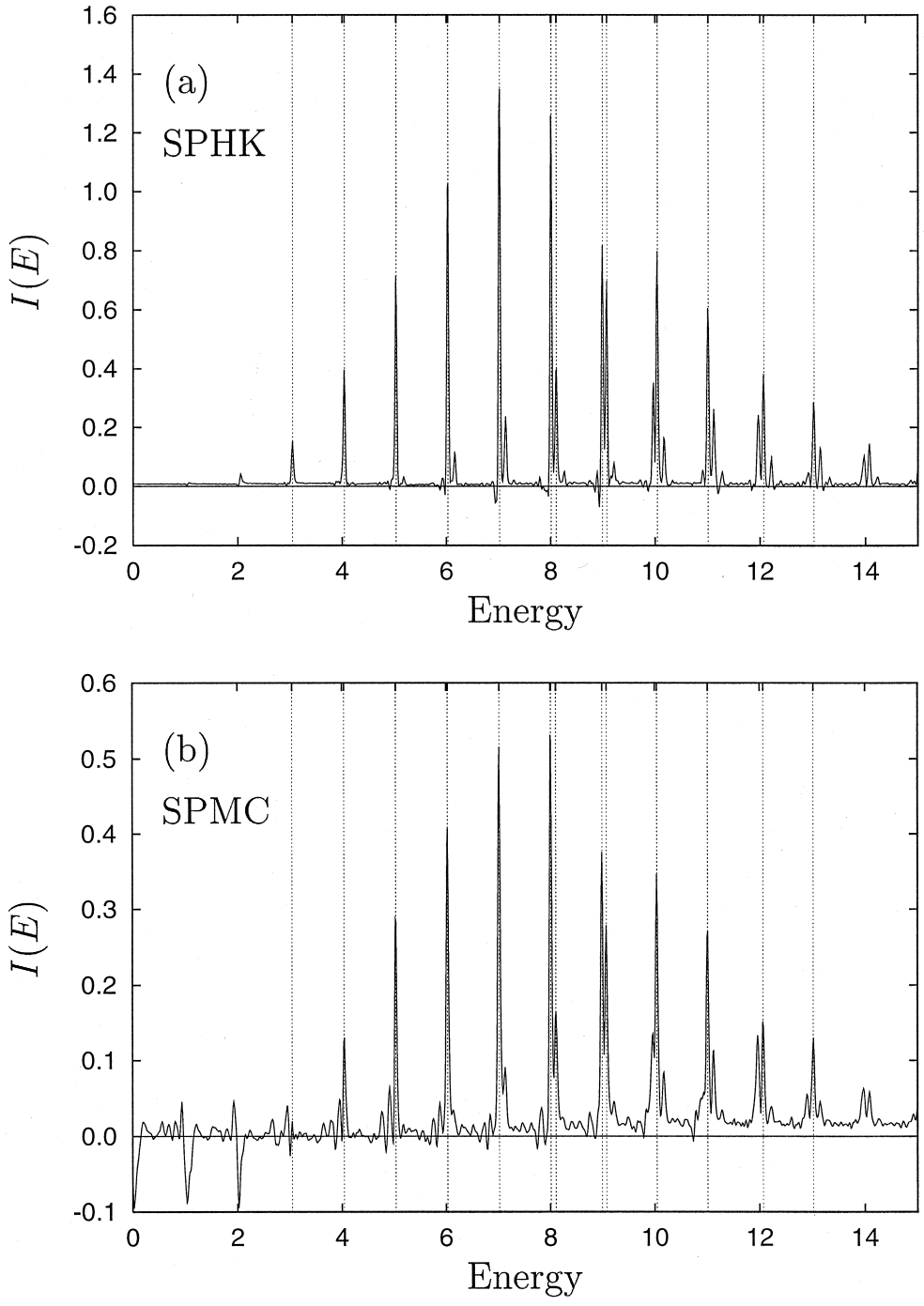

Fig. 1. HH Case 1. The vertical lines are some of the dominant quantum eigenvalues [6], although the additional peaks (above the noise) also reproduce the quantum result.

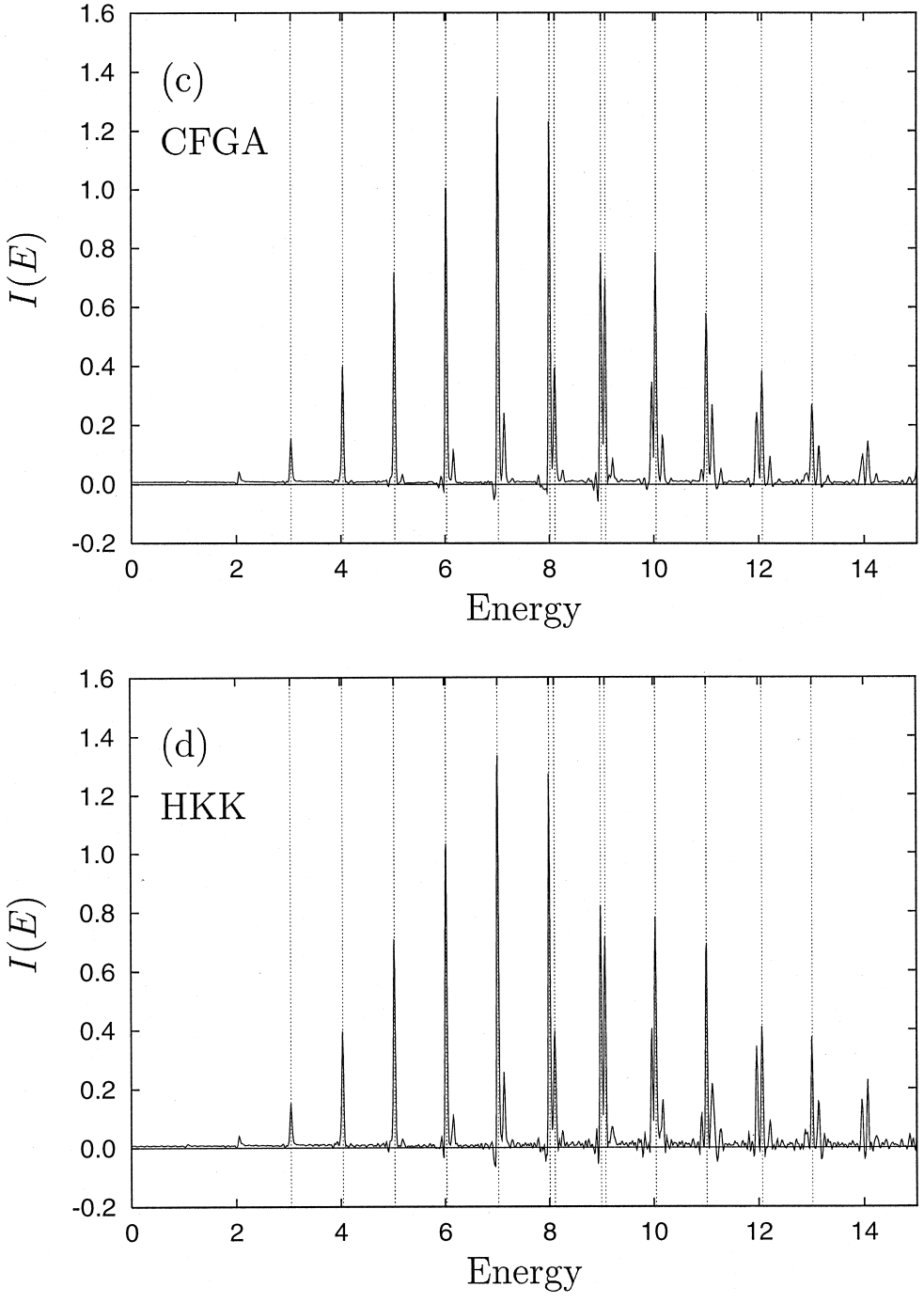

Fig. 1 (continued).

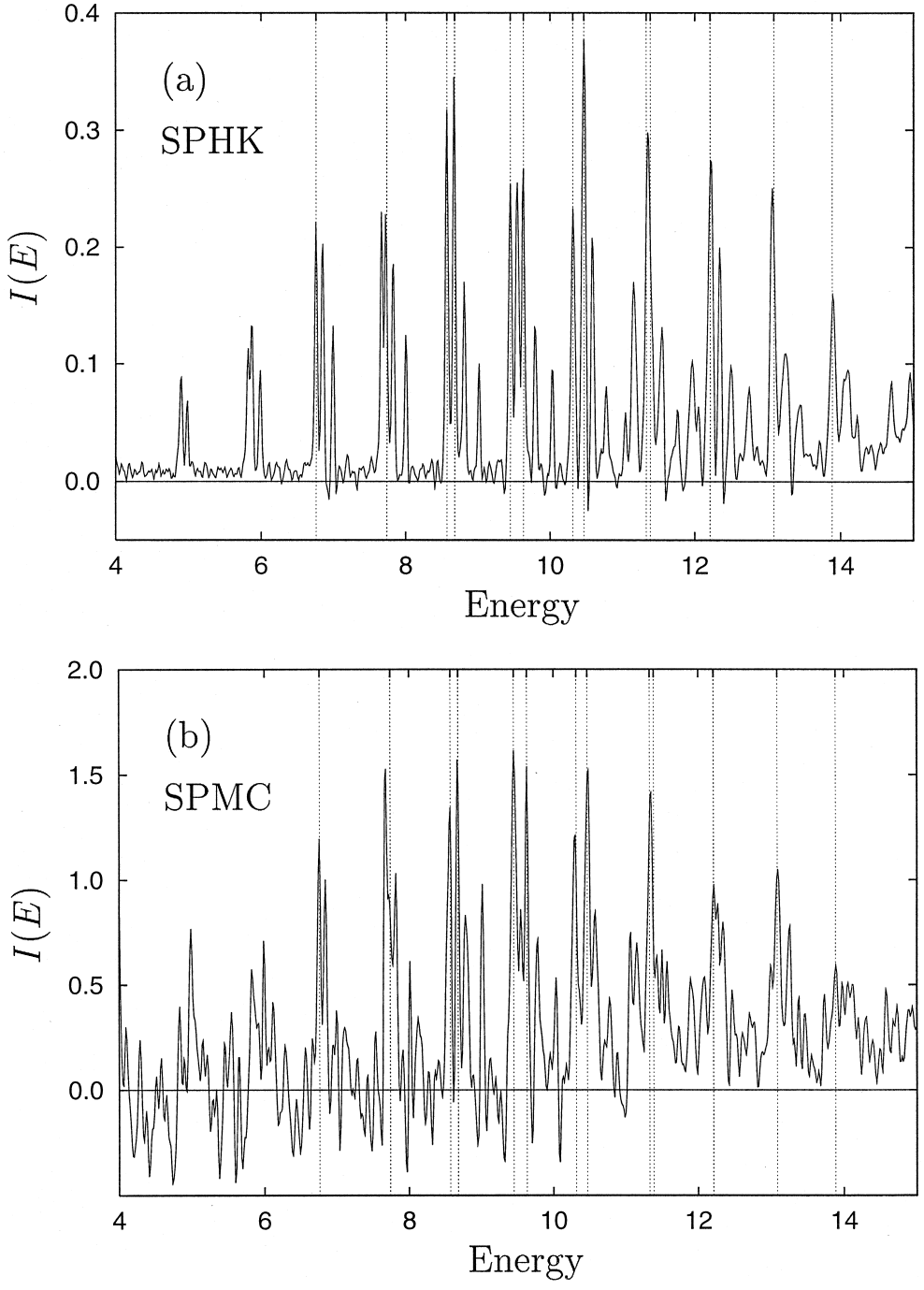

Fig. 2. HH Case 2. The vertical lines are some of the dominant quantum eigenvalues [6], although the additional peaks (above the noise) also reproduce the quantum result.

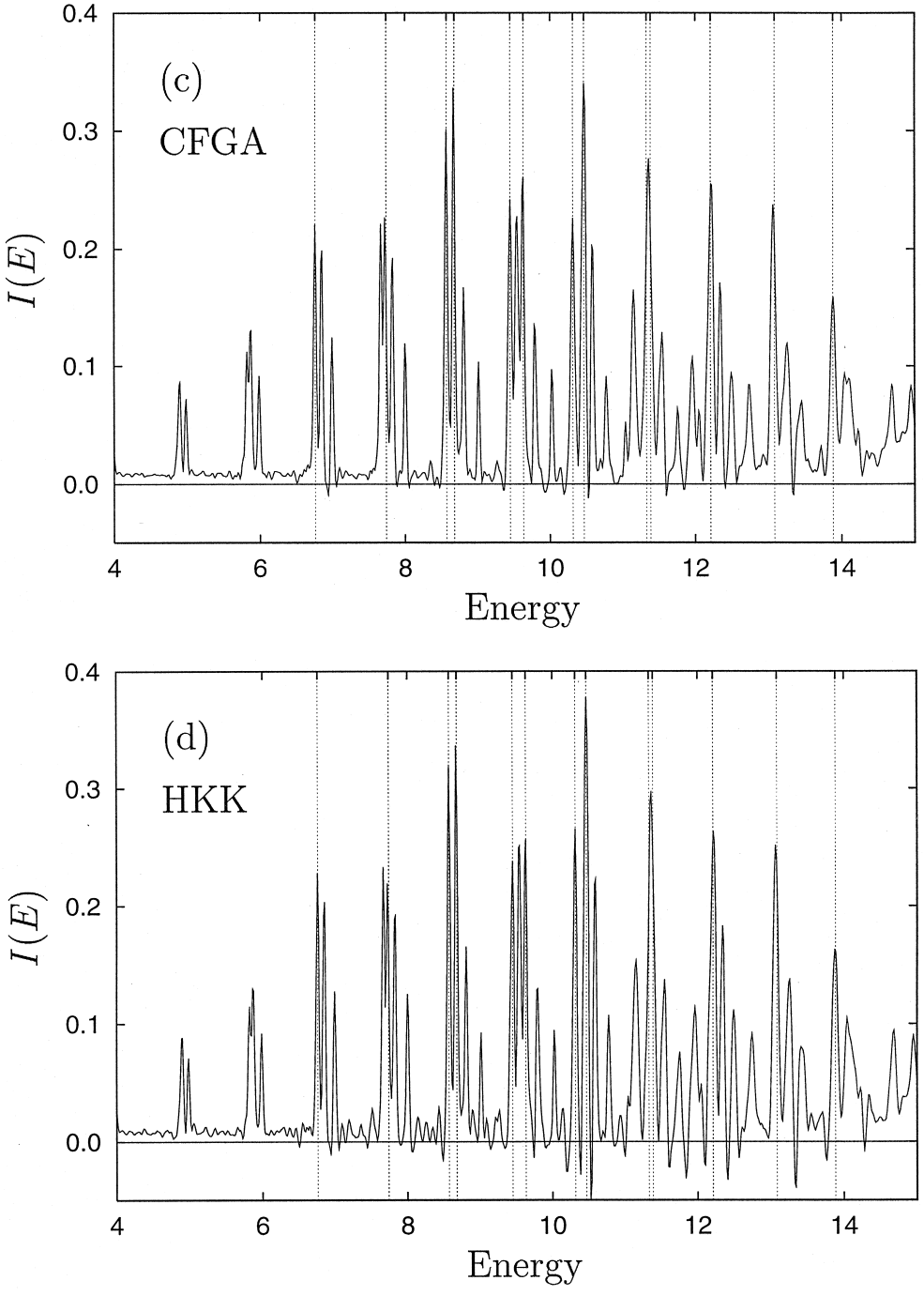

Fig. 2 (continued).

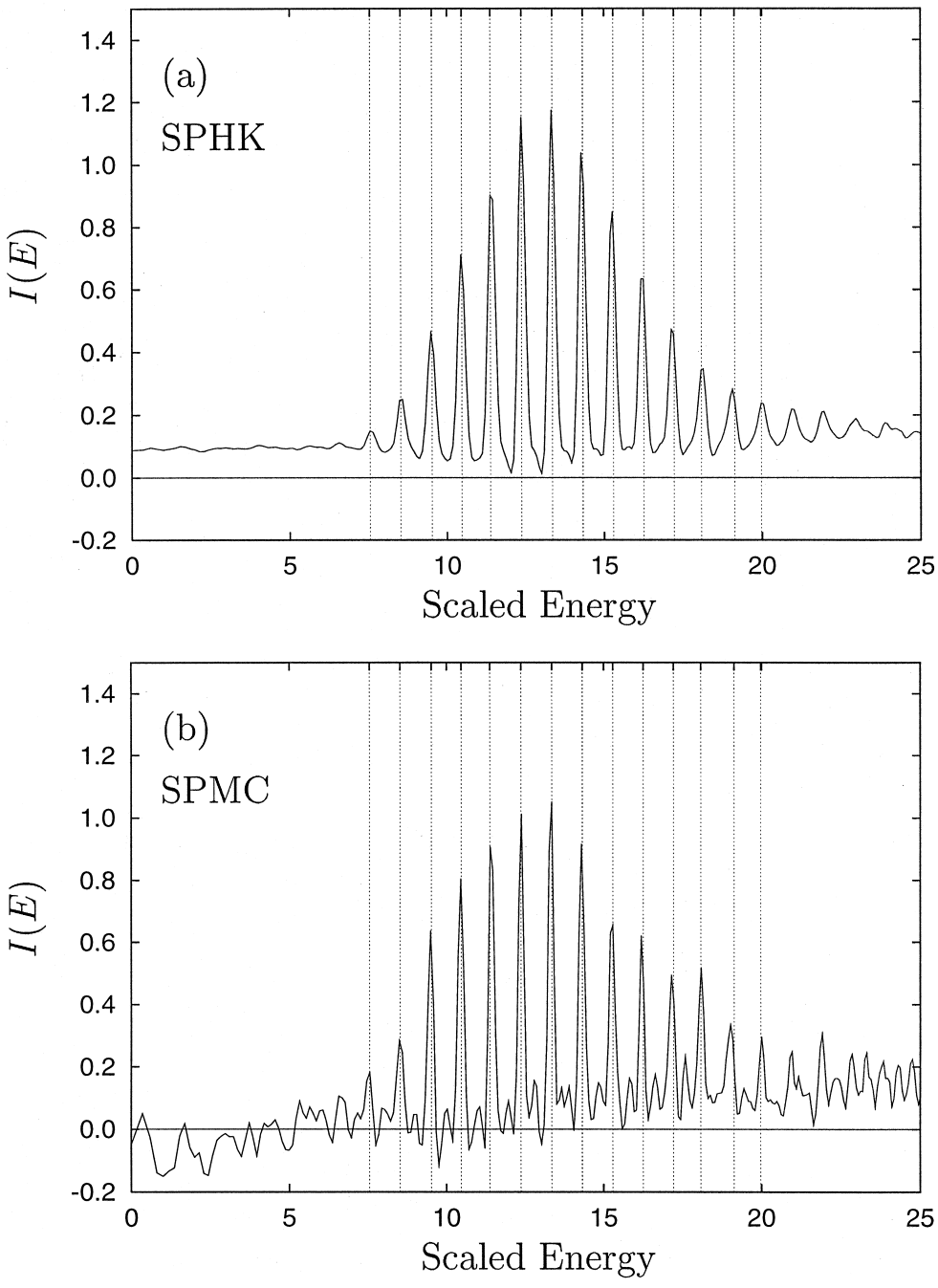

Fig. 3. Quartic oscillator. The vertical lines are some of the dominant quantum eigenvalues [28], although the additional peaks (above the noise) also reproduce the quantum result.

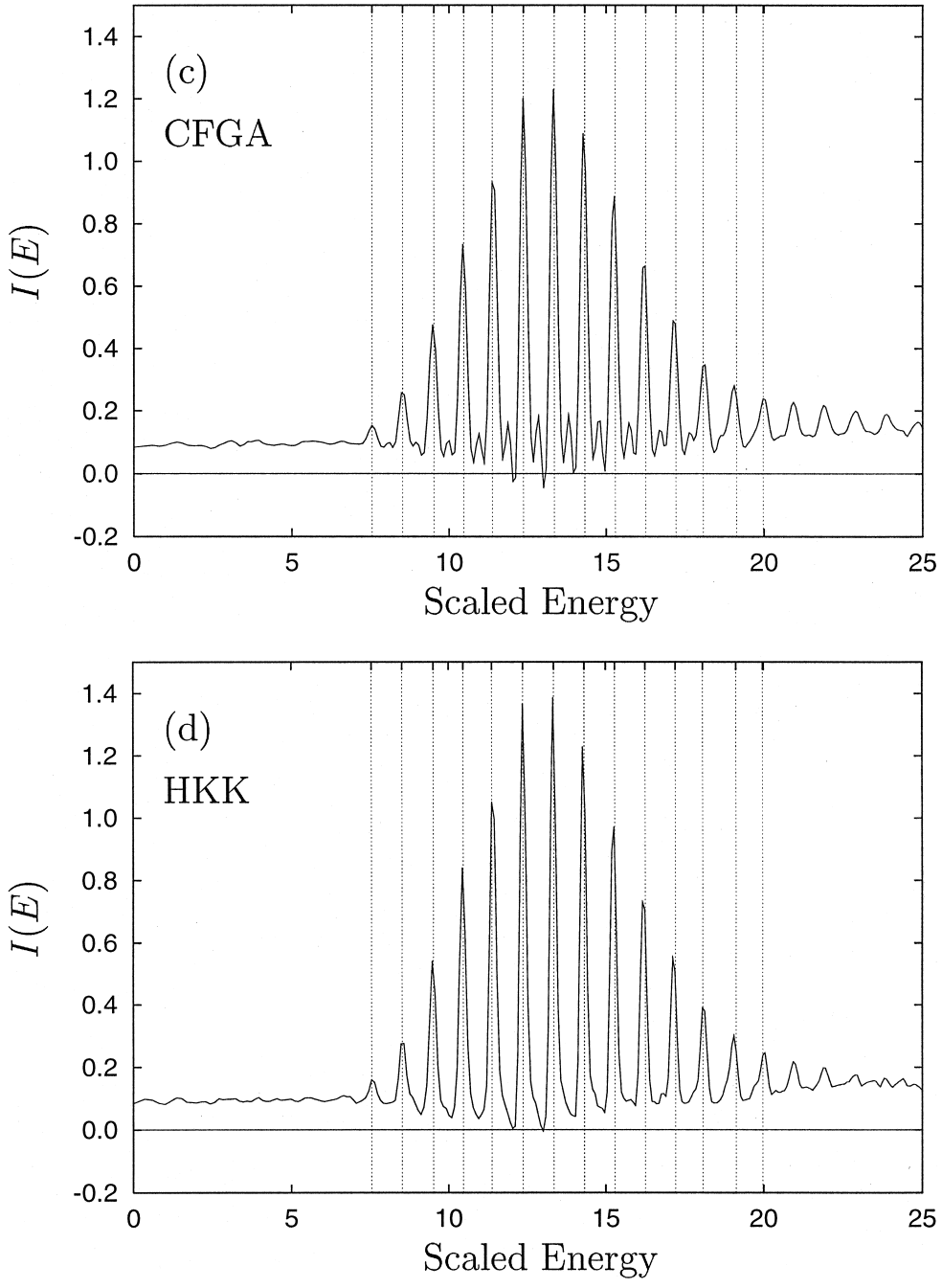

Fig. 3 (continued).

where ν is the Maslov index and the initial wavefunction is given by Eq. (2). Applying a stationary-phase procedure to Eq. (24) similar to that which generated Eq. (12) from Eq. (9), gives the sta-

tionary-phase Monte Carlo (SPMC) result (it is assumed that the Maslov index is constant within phase-space regions)

$$C^{\mathrm{sc}}_{\mathrm{SPMC}}(t) = \left(\frac{\alpha}{\pi^2 i\hbar}\right)^{d/2} \times \int\int \mathrm{d}\boldsymbol{p}\,\mathrm{d}\boldsymbol{q}\,|\det \boldsymbol{M}_{\boldsymbol{qp}}|^{1/2} \mathrm{e}^{iS_{\boldsymbol{p}\boldsymbol{q}t}/\hbar} \mathrm{e}^{i\pi\nu/2} \times D_{\boldsymbol{\epsilon p}\,\boldsymbol{q}t} \exp\left[-\alpha|\boldsymbol{q}-\bar{\boldsymbol{q}}|^2 - \alpha|\boldsymbol{q}(t)-\bar{\boldsymbol{q}}|^2 + i(\boldsymbol{q}(t)-\boldsymbol{q})\cdot\bar{\boldsymbol{p}}/\hbar\right], \tag{25}$$

where

$$D_{\boldsymbol{\epsilon p}\,\boldsymbol{q}t} = \exp\left\{-\frac{\boldsymbol{\epsilon}}{\hbar^2}\left[\left(\boldsymbol{M}_{\boldsymbol{qq}}\cdot(\boldsymbol{p}(t)+\bar{\boldsymbol{p}}) - (\boldsymbol{p}+\bar{\boldsymbol{p}})\right)^2 + \left(\boldsymbol{M}_{\boldsymbol{qp}}\cdot(\boldsymbol{p}(t)+\bar{\boldsymbol{p}})\right)^2\right]\right\}. \tag{26}$$

This result is quite different from the methods based on Herman–Kluk. In particular, the $\boldsymbol{p}$ and $\boldsymbol{q}$ are treated differently in this equation. Specifically the $\boldsymbol{p}$ integration does not benefit from a Gaussian decay factor. In addition, the $t \to 0$ limit of Eq. (24) is not obvious (it does, in fact, reproduce the result $C^{\mathrm{sc}}(0) = 1$ [5]). These two considerations are drawbacks of the SPMC method.

The differences between the stationary-phase conditions for SPHK and SPMC should also be noted. For SPHK, the phase contains a momentum dependence which is not in the SPMC. This results in a stationary-phase term (Eq. (13)) which is more symmetric in coordinate and momentum than that for SPMC (Eq. (26)). The SPHK is therefore expected to be better at damping down regions of phase space which contribute a negligible amount to the integral.

3. Results and discussion

3.1. Essentially bound systems

In Section 3.1, we compare results for these four semiclassical IVR methods as applied to increasingly chaotic 2-dimensional bound-state systems. In each case, the IVR integrals are evaluated by Monte Carlo integration. A box Muller transformation [24] is used to perform the $\boldsymbol{p}$ and $\boldsymbol{q}$ integrals for the HK-based methods (HKK, CFGA, SPHK), and the $\boldsymbol{q}$ integral in the SPMC method. The $\boldsymbol{p}$ integral in the SPMC method is carried out using a simple Monte Carlo method over a rectangular region. The spectra are found from the autocorrelation function by an FFT [24], and are artificially broadened to be consistent with previous treatments using a windowing function $W(t) = \exp[-t^2/(2W_T^2)]$.

We consider two cases, a modified HH Hamiltonian and a quartic oscillator, where the Hamiltonian $H = (1/2)\boldsymbol{p}^2 + V(\boldsymbol{q})$ and where $\hbar = 1$. The modified 2-dimensional HH system [25] has the potential

$$V(q_x, q_y) = \tfrac{1}{2}w_x^2 q_x^2 + \tfrac{1}{2}w_y^2 q_y^2 + \lambda q_x^2 q_y - \mu q_y^3. \tag{27}$$

We consider two parameter sets [1,6]: Case 1 has $w_x = 1.1$, $w_y = 1$, $\lambda = -0.11$, $\mu = 0.0$, $\alpha = 0.5$, $\bar{q}_x = 0$, $\bar{q}_y = 4$, $\bar{\boldsymbol{p}} = 0$, $W_T = 57.0$; Case 2 has $w_x = w_y = 1$, $\lambda = 0.111803$, $\mu = 0.037268$, $\alpha = 0.5$, $\bar{q}_x = 0$, $\bar{q}_y = -1.914$, $\bar{p}_x = 3.976$, $\bar{p}_y = 0.961$, $W_T = 57.0$. The average Lyapunov exponents for the two cases are 0.2 and 0.16, respectively. That is, these systems are only mildly chaotic. The systems have dissociative classical trajectories above $E_d \sim 15.125$ and 13.333, respectively. Such trajectories are included in the phase-space average only up until the time of dissociation. The final time is taken as $T = 450$.

The quartic oscillator, which is much more chaotic than the HH potential [26,27], has [28]

$$V(q_x, q_y) = \tfrac{1}{2}q_x^2 q_y^2 + \frac{\beta}{4}\left(q_x^4 + q_y^4\right), \tag{28}$$

with [12] $\beta = 0.01$, $\alpha = 0.5$, $\bar{q}_x = 0$, $\bar{q}_y = 8.32$, $\bar{\boldsymbol{p}} = 0, W_T = 17.7$. For the quartic oscillator, the results are presented in terms of the scaled energy, $(2E)^{3/4}$ [28]. In this case, the average Lyapunov exponent is 0.8, which is an order of magnitude larger than for the least chaotic HH case considered. Since the

Table 2
Average Lyapunov exponent and number of trajectories to converge the spectrum using the SPHK method

	λ	No. of trajectories
HH Case 1	0.02	2000
HH Case 2	0.16	40000
Quartic Case 2[a]	0.83	100000
Quartic Case 1	0.93	100000

[a] $\beta = 0.01, \alpha = 2.0, \bar{q}_x = 0, \bar{q}_y = 5.0, \bar{p}_x = 5.0, \bar{p}_y = 0, \epsilon = 10^{-6}$.

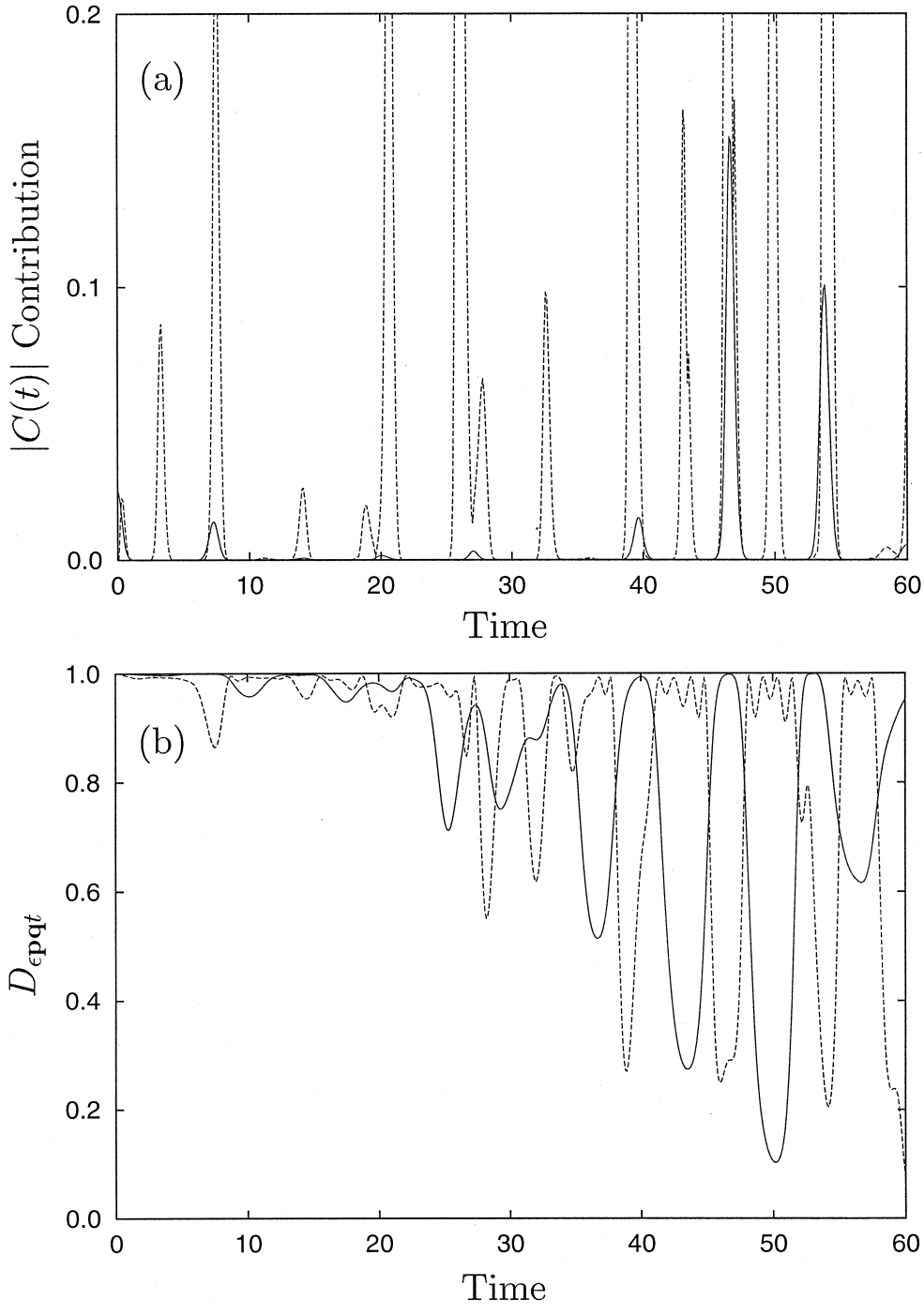

Fig. 4. (a) Single trajectory contributions to $|C(t)|$ and (b) the stationary-phase damping term ($D_{\epsilon p\, q t}$) with $\epsilon = 10^{-7}$ for HH Case 2 (Eqs. (13) and (26)); solid lines are SPHK, dashed lines are SPMC. The initial conditions for the trajectory are $\boldsymbol{q} = \bar{\boldsymbol{q}}, \boldsymbol{p} = \bar{\boldsymbol{p}}$. For ease of comparison, the $D_{\epsilon p\, q t}$ term is not included in the $|C(t)|$ contribution.

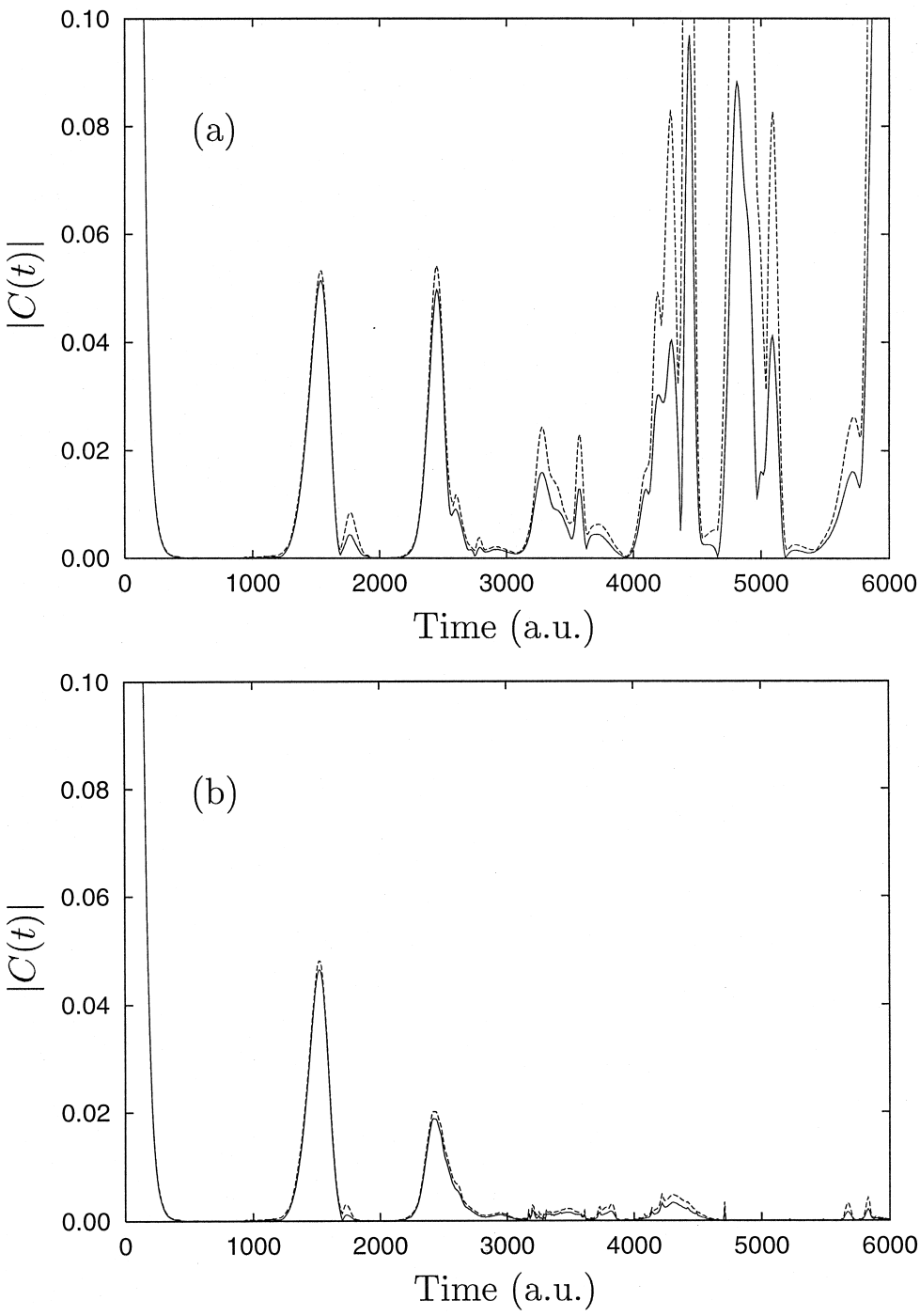

Fig. 5. Results for CO_2 photodissociation with 10^6 trajectories: (a) HK autocorrelation, dashed line is one standard deviation error in the Monte Carlo sum; (b) SPHK autocorrelation with $\epsilon = 10^{-7}$; (c) HK spectrum (dash) and SPHK spectrum (solid).

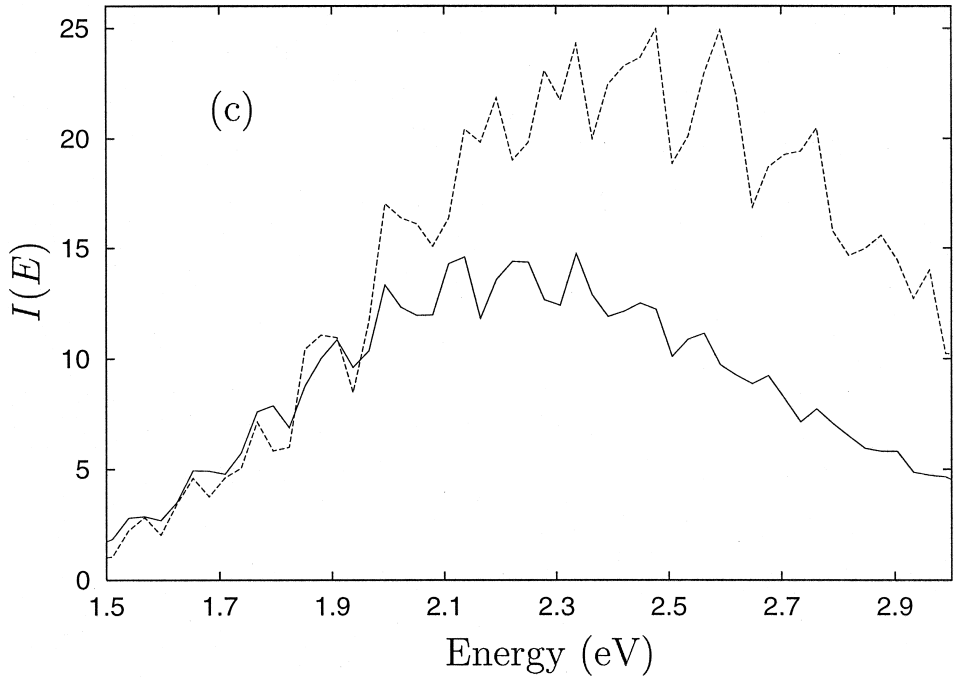

Fig. 5 (continued).

quartic oscillator is a confining potential, no trajectories dissociate. The final time is taken as $T = 50$.

The quartic oscillator posseses C_{4v} symmetry [29], and we only consider states with A_1 symmetry, i.e. wavefunctions which are symmetric under reflections across the axes and symmetric under reflections across the diagonals. An arbitrary function G can be modified in the following manner to satisfy A_1 symmetry

$$\begin{aligned}\hat{p}_{A_1} G\left(\bar{q}_x,\bar{p}_x,\bar{q}_y,\bar{p}_y\right) &= G\left(\bar{q}_x,\bar{p}_x,\bar{q}_y,\bar{p}_y\right) + G\left(-\bar{q}_y,-\bar{p}_y,\bar{q}_x,\bar{p}_x\right) \\ &\quad + G\left(\bar{q}_y,\bar{p}_y,-\bar{q}_x,-\bar{p}_x\right) \\ &\quad + G\left(-\bar{q}_x,-\bar{p}_x,-\bar{q}_y,-\bar{p}_y\right) \\ &\quad + G\left(-\bar{q}_x,-\bar{p}_x,\bar{q}_y,\bar{p}_y\right) \\ &\quad + G\left(\bar{q}_x,\bar{p}_x,-\bar{q}_y,-\bar{p}_y\right) \\ &\quad + G\left(\bar{q}_y,\bar{p}_y,\bar{q}_x,\bar{p}_x\right) \\ &\quad + G\left(-\bar{q}_y,-\bar{p}_y,-\bar{q}_x,-\bar{p}_x\right). \end{aligned} \tag{29}$$

Thus, our initial Gaussian wavefunction is replaced by the sum of eight Gaussians.

Table 1 contains the values of the adjustable parameters, the number of trajectories, the average final time (t_f) of the trajectories, and the percent of trajectories truncated for each of the cases studied. Note that although the CFGA method does not explicitly call for discarding trajectories, we found that the complex matrix manipulations required the truncation of trajectories in order to obtain results (these matrix manipulations have previously been noted as a possible weakness, confirmed herein, by Garashchuk and Tannor [9]). Specifically, we found that for some chaotic trajectories the matrix $A_{\boldsymbol{p}\,\boldsymbol{q}t}$ would grow to such a size as to make inversion inaccurate. If these trajectories were not truncated then the integrand grew to infinity and the results became meaningless. Note also that the data in Table 1 makes clear that the SPMC method requires 2–5 times the number of trajectories than does the HK-based methods to achieve convergence.

The resultant $I(E)$ for all cases is shown in Figs. 1 and 3. The results are all in good agreement with

the quantum $I(E)$ [6,12] except for the extra noise seen in the SPMC results. Further, a comparison of the $I(E)$ in Figs. 1 and 3 makes clear that all the HK-based methods are in basic agreement with one another. By contrast, the SPMC results are somewhat noisier even though the method utilizes more trajectories.

Table 2 shows a comparison of the Lyapunov exponent and the number of trajectories required for convergence. Clearly, increasing λ necessitates a larger trajectory sample. As is evident from Fig. 3, however, the system with the largest λ need not display the most chaotic spectrum (compare Fig. 2 and Fig. 3). Rather, in the case of the quartic oscillator, a large number of trajectories had to be run in order to expose the underlying, simple autocorrelation function. Indeed, for the quartic oscillator the HKK methods obtains results with only very short time trajectories. This is because the correct quartic oscillator autocorrelation function is quasiperiodic, so that a nearly correct spectrum would result from a computation over a single period. This is not, however, a general result. For example, the HH system requires the proper computation of a large number of resonances since the autocorrelation function is not quasiperiodic.

Also of interest is the extent to which spectral results can be obtained with a small number of trajectories. In general, the spectrum which results from using fewer trajectories is noisier. However, in many cases it is possible to determine the eigenvalues to sufficient accuracy with far fewer trajectories than reported in Table 1. For example, all HK-based methods gave good results for the HH Case 1 with as few as 500 trajectories. Similarly, the SPHK quartic oscillator spectrum ($\epsilon = 10^{-6}$) can be estimated quite accurately using only 10^4 trajectories. However, convergence is only attained with 10^5 trajectories.

Finally, we comment on the inefficiency of the SPMC method. This is due to the lack of localization of the $\boldsymbol{p}$ integration. That is, since the integrand does not contain localizing terms of the form $\exp[-\xi(\boldsymbol{p}-\bar{\boldsymbol{p}})^2]$ or $\exp[-\xi(\boldsymbol{p}(t)-\bar{\boldsymbol{p}})^2]$, the SPMC relies to a greater degree on numerical cancellation than do the HK methods. For example, Fig. 4 shows the difference in single trajectory contributions to the SPMC and the SPHK methods. Specifically, the single trajectory contribution to the autocorrelation (Fig. 4a) is seen to be both much larger and have more peaks for the SPMC. Some of these peaks will have to be cancelled by contributions from other trajectories in order to obtain a near zero result, which the SPHK obtains automatically. The stationary-phase damping term $D_{\epsilon pqt}$ (Fig. 4b) is also seen to be smoother and spends less time near unity for the SPHK, due to the extra terms in Eq. (13) which are not present in Eq. (26). The stationary-phase procedure therefore achieves better damping of chaotic trajectories for the SPHK than it does for the SPMC.

3.2. Photodissociation

Our particular interest is in the use of IVR techniques for coherent control [30] and hence for processes like photodissociation. Previous studies of 3D photodissociation using the SPMC method [31] showed good results but required many trajectories. In an effort to see the utility of other IVR methods we consider collinear CO_2, a system which has been previously examined in great detail [11,32–34]. In particular, we compare the HK and SPHK approaches to explore the effect of the stationary-phase method. CO_2 provides an interesting case because its spectrum depends heavily on a relatively small number of periodic orbits [33,34]. For example, Walton and Manolopoulos studied collinear CO_2 using the HK formalism [11], and required 10^8 trajectories for convergence, due to both periodic orbits (specifically, the symmetric stretch motion), as well as the dissociative nature of the system. Here we extend the SPHK to photodissociation and demonstrate substantially improved efficiency over the HK approach.

The model CO_2 Hamiltonian is given by [33]

$$H = \frac{1}{2\mu}\boldsymbol{p}^2 - \frac{1}{m_C}p_1 p_2 + V(R_1, R_2) \tag{30}$$

where R_1 and R_2 are CO and OC interatomic distances, and $\mu = m_O m_C/(m_O + m_C)$. The potential used is the LEPS potential [35], parameters are taken from Ref. [32], and energy is measured relative to CO_2 dissociation. The initial state of the system is given by Eq. (2), with equilibrium separation $R_e = \bar{q}_1 = \bar{q}_2 = 2.20\ a_0$, $\bar{\boldsymbol{p}} = 0$ a.u., $\alpha = 69.2\ a_0^{-2}$. The CO_2 spectrum was computed with $\epsilon = 10^{-7}$ from

the autocorrelation function with no windowing function.

Fig. 5 shows the autocorrelation and spectrum obtained using 10^6 trajectories for both the HK and the SPHK methods. As can be seen from Fig. 5a, the HK autocorrelation has not converged for large times, resulting in an inaccurate representation of the spectrum (Fig. 5c). By contrast, the SPHK autocorrelation is well converged (Fig. 5b), and the associated spectrum is in good agreement with quantum results [32], allowing for accurate estimates of the energy eigenvalues (Fig. 5c). Thus, the autocorrelation and associated eigenvalues can be estimated using the SPHK with two orders of magnitude fewer trajectories than that required by the HK method.

The extent to which this spectrum agrees with the true quantum spectrum was found to depend greatly on the choice of ϵ. If ϵ is chosen too large, important long time information can be lost (cf. Section 2). Note, however, that even though the autocorrelation in Fig. 5b does not contain the actual structure of the correct CO_2 autocorrelation for times greater than 3000 a.u. (due to an insufficient number of trajectories), it does contain enough of the actual autocorrelation structure to provide good results for the photodissociation spectrum (computed from all time points). This is largely due to the simplicity of the CO_2 autocorrelation.

Finally, since periodic orbits are important in the CO_2 system, we note the effect of the stationary-phase procedure on periodic orbits. For the important symmetric stretch periodic orbits in the CO_2 system, $D_{\epsilon \boldsymbol{p}\boldsymbol{q}t} \sim 1$ for $\epsilon = 10^{-7}$, so the SPHK procedure includes the symmetric stretch effects which are essentially unmodified from the HK results. This is quite different from a HKK treatment which would have discarded the trajectory once the prefactor $R_{\boldsymbol{p}\boldsymbol{q}t}$ became large. Trajectories which return to the Frank–Condon region but which are far from periodic have $D_{\epsilon \boldsymbol{p}\boldsymbol{q}t} \sim 0$.

4. Conclusions

We have applied four semiclassical IVR methods to a number of chaotic systems, in order to determine the method with best overall performance. All methods gave reasonable spectra but differed in utility.

The SPMC method required more trajectories than any of the HK-based results, due to the lack of a Gaussian damping function on the $\boldsymbol{p}$ integral in Eq. (24). Further, the noise in the resultant $I(E)$ was considerable, and an expression which is not numerically tractable at $t = 0$ made this the least effective method of those studied.

The CFGA method also suffers from numerical difficulties involving matrix inversion when the trajectories are chaotic. It required the truncation of trajectories, a procedure which we prefer to avoid.

The HKK is still seen to be a good method for chaotic systems, although the trajectory truncation procedure remains unsatisfying. Nonetheless, this relatively simple method was able to provide results which matched the quality of the more numerically ambitious methods.

The most successful of the four methods for calculating the bound-state Frank–Condon spectrum is the SPHK. It produced accurate results and did not require the truncation of any trajectories. It also produced good estimates of the spectrum for collinear CO_2 photodissociation and required a relatively small number of trajectories. The SPHK is able to determine the autocorrelation for chaotic systems very accurately, and requires only a small amount of numerical calculation beyond that of the HK method. Further, the SPHK method is such that if greater accuracy is required one can decrease the smoothing parameter ϵ giving a result approaching that of the converged HK method. The ability of SPHK to give reasonable results for a small number of trajectories is useful for initial treatments of systems, and also allows some systems to be solved accurately using only modest computing power.

The HK-based methods were found to be especially well suited to the problem studied, where the overlap of the initial and time-evolved wavefunction is calculated. However, if one wishes to calculate the propagated wavefunction, then we note that HK-based methods require an integration over the full-phase space $(\boldsymbol{q}, \boldsymbol{p})$, whereas the SPMC requires only an integration over $\boldsymbol{q}$-space. This extra integration may prove advantageous: Kay has shown [4], by calculating the overlap of the semiclassical wavefunction with the quantum wavefunction, that the HK for non-chaotic systems (and the HKK for chaotic systems [12]) produce very accurate propagated

wavefunctions. These results suggest that HK-based methods like the SPHK should be useful in obtaining more detailed properties of the system (such as photofragmentation matrix elements) which do not rely on an overlap with the initial state. Work in this direction is in progress.

Acknowledgements

The authors would like to thank Prof. Ken Kay (Bar-Ilan University) for a helpful communication regarding symmetry adaption for the quartic oscillator potential. This work was supported by the US Office of Naval Research and by the Natural Sciences and Engineering Research Council of Canada.

References

[1] E.J. Heller, J. Chem. Phys. 75 (1981) 2923.
[2] M.F. Herman, E. Kluk, Chem. Phys. 91 (1984) 27.
[3] K.G. Kay, J. Chem. Phys. 100 (1994) 4377.
[4] K.G. Kay, J. Chem. Phys. 100 (1994) 4432.
[5] G. Campolieti, P. Brumer, Phys. Rev. A 50 (1994) 997.
[6] A.R. Walton, D.E. Manolopoulos, Mol. Phys. 87 (1996) 961.
[7] M.F. Herman, Chem. Phys. Lett. 275 (1997) 445.
[8] J.H. Van Vleck, Proc. Natl. Acad. Sci. USA 14 (1928) 178.
[9] S. Garashchuk, D. Tannor, Chem. Phys. Lett. 262 (1996) 477.
[10] G. van de Sand, J.M. Rost, Phys. Rev. A. Rapid Comm. 59 (1999) R1723.
[11] A.R. Walton, D.E. Manolopoulos, Chem. Phys. Lett. 244 (1995) 448.
[12] K.G. Kay, J. Chem. Phys. 101 (1994) 2250.
[13] G. Campolieti, P. Brumer, J. Chem. Phys. 109 (1998) 2999.
[14] E.J. Heller, J. Chem. Phys. 68 (1978) 2066.
[15] E.J. Heller, J. Chem. Phys. 94 (1991) 2723.
[16] B.E. Guerin, M.F. Herman, Chem. Phys. Lett. 286 (1998) 361.
[17] N. Makri, W.H. Miller, Chem. Phys. Lett. 139 (1987) 10.
[18] N. Makri, W.H. Miller, J. Chem. Phys. 89 (1988) 2170.
[19] B.W. Spath, W.H. Miller, J. Chem. Phys. 104 (1996) 95.
[20] V.S. Batista, W.H. Miller, J. Chem. Phys. 108 (1998) 498.
[21] V.S. Filinov, Nucl. Phys. B 271 (1986) 717.
[22] M.L. Brewer, J.S. Hulme, D.E. Manolopoulos, J. Chem. Phys. 106 (1997) 4832.
[23] J. Cao, G.A. Voth, J. Chem. Phys. 104 (1996) 273.
[24] W.H. Press, S.A. Teukolsky, W.T. Vetterling, B.P. Flannery, Numerical Recipes: the Art of Scientific Computing, 2nd edn., Cambridge University Press, Cambridge, 1996.
[25] M. Hénon, C. Heiles, Astron. J 69 (1964) 73.
[26] H.D. Meyer, J. Chem. Phys. 84 (1986) 3147.
[27] A. Carnegie, I.C. Percival, J. Phys. A 17 (1983) 801.
[28] B. Eckhardt, G. Hose, E. Pollak, Phys. Rev. A 39 (1989) 3776.
[29] F.A. Cotton, Chemical Applications of Group Theory, Wiley–Interscience, New York, 1971.
[30] M. Shapiro, P. Brumer, Adv. Atomic Mol. Opt. Phys. 42 (2000) 287.
[31] G. Campolieti, P. Brumer, J. Chem. Phys. 107 (1997) 791.
[32] K.C. Kulander, J.C. Light, J. Chem. Phys. 73 (1980) 4337.
[33] R. Schinke, V. Engel, J. Chem. Phys. 93 (1990) 3252.
[34] K.C. Kulander, C. Cerjan, A.E. Orel, J. Chem. Phys. 94 (1991) 2571.
[35] S. Sato, J. Chem. Phys. 23 (1955) 592.